Manifestation of postcollision interaction in Krypton *LMN* Auger spectra following *K*-shell photoionization

S. Li,[1] D. Koulentianos [ID],[1,*] S. H. Southworth [ID],[1,†] G. Doumy,[1] L. Young [ID],[1,2] D. A. Walko,[3] R. Püttner [ID],[4] J. D. Bozek,[5]
D. Céolin,[5] A. Verma [ID],[6] R. Guillemin,[6] M. N. Piancastelli,[6,7] M. Simon [ID],[6] L. G. Gerchikov [ID],[8] and S. A. Sheinerman [ID][9]

[1]*Chemical Sciences and Engineering Division, Argonne National Laboratory, Lemont, Illinois 60439, USA*
[2]*The James Franck Institute and Department of Physics, The University of Chicago, Chicago, Illinois 60637, USA*
[3]*Advanced Photon Source, Argonne National Laboratory, Lemont, Illinois 60439, USA*
[4]*Fachbereich Physik, Freie Universität Berlin, Arnimallee 14, D-14195 Berlin, Germany*
[5]*Synchrotron SOLEIL, l'Orme des Merisiers, Saint-Aubin, BP 48, 91192 Gif-sur-Yvette, France*
[6]*Sorbonne Université, CNRS, Laboratoire de Chimie Physique-Matière et Rayonnement, LCPMR, F-75005 Paris, France*
[7]*Department of Physics and Astronomy, Uppsala University, SE-75120 Uppsala, Sweden*
[8]*Department of Physics, Peter the Great St. Petersburg Polytechnic University, 195251 St. Petersburg, Russia*
[9]*Department of Physics, St. Petersburg State Marine Technical University, 190121 St. Petersburg, Russia*

We report on an experimental and theoretical study of postcollision interaction (PCI) effects on $L_2 - M_{4,5}N_{2,3}$ Auger electrons measured above the Kr K-edge in which L_2 vacancies are primarily generated by KL_2 x-ray emission. Such cascade processes, in which a deep inner-shell vacancy decays first by x-ray emission followed by Auger electron emission, is a strong decay mode in heavy atoms. The $L_2 - M_{4,5}N_{2,3}$ Auger electron peak is observed to become increasingly asymmetric with a shifting peak maximum as the absorbed x-ray energy approaches the K-shell ionization threshold. This is attributed to PCI energy exchanges of the Auger electron with the $1s$ photoelectron. To model the PCI effects, we have applied a semiclassical approach modified to account for the combined lifetimes of the K and L_2 hole states. In addition, our analysis treats several closely spaced Auger transitions with final ionic states having different terms and angular momenta.

I. INTRODUCTION

Postcollision interaction (PCI) in atomic inner-shell photoionization has been extensively investigated during the last several decades (see, e.g., Refs. [1–3] and references therein). Interest in this subject is motivated by the need for understanding the complicated dynamics of deep shell vacancy decay. PCI is associated with the Coulomb interaction between the emitted electrons and the receding ion and strongly influences the energy distributions of the photoelectrons and the Auger electrons. PCI effects have largely been studied in processes where the initially created vacancy decays by means of single Auger decay [4–6] or double Auger decay [4,7–10].

An alternative decay pathway is by radiative decay of the initial core hole, a process of increasing importance for K-shell vacancies of heavy atoms since the fluorescence yields increase rapidly with the atomic number Z [11]. In this case, an electron from an intermediate shell fills the deep vacancy and a high-energy photon is emitted. Such a radiation process can be followed by Auger decay of the intermediate vacancy. PCI effects are also revealed in these consequent radiation-Auger decay (CRAD) processes and lead to distortions of the

photoelectron spectra and the Auger electron spectra. These effects were first observed in the slow (2–4 eV) photoelectron spectra recorded in coincidence with selected charge states of the receding ion for the case of Ar $1s$ photoionization [8]. The PCI distortion of the emitted *LMM* Auger electron spectra for the same case of Ar $1s$ photoionization followed by CRAD processes has been studied in noncoincidence measurements [12]. The CRAD process was also investigated in PCI distortion of the $L_3 - M_{4,5}M_{4,5}$ Auger line following Kr $1s$ photoionization for a few values of excess photon energy above the threshold [13]. However, no systematic study of the PCI effects in CRAD processes following deep shell photoionization over a wide range of photon energies has yet been carried out.

Here we present results of PCI distortion of the Kr $L_2 - M_{4,5}N_{2,3}$ Auger electron line emitted in the CRAD process following $1s$ photoionization. The Auger decay considered demonstrates effects with the following distinguishing features:

(1) The PCI distortion of the energy distribution of the emitted electrons, i.e., the shift and asymmetry of the line shape, depends strongly on the widths of the initially created K vacancy and the L_2 vacancy which decays with Auger electron emission. Such a distortion increases with the widths of the vacancy states. The widths of the vacancies involved in the case considered here in Kr are large: ($\Gamma(1s) = 2.75$ eV, $\Gamma(L_2) = 1.31$ eV [14]). Hence, one can expect a significant PCI effect.

---

*Present address: Center for Free-Electron Laser Science and Department of Physics, Universität Hamburg, Luruper Chaussee 149, 22761 Hamburg, Germany.
†Corresponding author: southworth@anl.gov

(2) The electron spectrum of the $L_2 - M_{4,5}N_{2,3}$ Auger transition includes several lines with different total angular momenta [15]. In Ref. [15], the Kr L-shell Auger electron spectra have been investigated in detail experimentally and theoretically. The calculated Auger transition energies and decay rates are tabulated in the Supplemental Material of Ref. [15]. The energies of these lines overlap and span a rather narrow interval ~ 3 eV. Hence, all these lines can contribute to the measured yield of the Auger electrons if the exact final state of the Auger transition is not resolved in the experiment. Each line is essentially affected by PCI. So, the measured electron yield is formed by the combined contributions of the individual lines. Hence, the measured line shape differs from the traditional line shape distorted by PCI effects and requires an additional analysis.
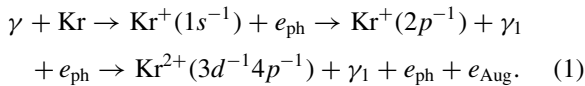
(3) The $L_2 - M_{4,5}N_{2,3}$ transition was chosen for investigation of PCI effects since it is relatively well isolated from other transitions, which makes its line shape analysis more clear.

Using tunable x rays and electron spectroscopy, we have measured the energy position and line shape of the Kr $L_2 - M_{4,5}N_{2,3}$ Auger transition over a wide range of incident photon energies, from the $1s$ threshold to several hundred eV excess energy. In the near-threshold region, strong PCI distortion has been observed, namely, we have observed a significant energy shift of the line and a remarkable asymmetrical line shape. The PCI effects have also been calculated within the modified quasiclassical approach [8]. The PCI shift calculations agree rather well with the measurements. Also, analysis and calculation of the PCI distorted line shapes show that the measured line shapes are formed from contributions of several individual PCI distorted Auger transitions.

Our paper is organized as follows: In Sec. II, we give a short description of the CRAD process and the theoretical approach used in this paper; in Sec. III, we describe the experimental setup used to measure the Auger spectra presented in the paper; and in Sec. IV, we compare and discuss the results of measurements and calculations of the PCI influence on the shapes and energy positions of the Auger lines. The atomic system of units, $|e| = m_e = \hbar = 1$, is used throughout unless otherwise indicated.

II. CRAD PROCESS OF INNER VACANCY

We will consider the process of Krypton $1s^2$ photoionization followed by CRAD of the inner vacancy. The scheme of the process is

$$\gamma + \text{Kr} \rightarrow \text{Kr}^+(1s^{-1}) + e_{\text{ph}} \rightarrow \text{Kr}^+(2p^{-1}) + \gamma_1$$
$$+ e_{\text{ph}} \rightarrow \text{Kr}^{2+}(3d^{-1}4p^{-1}) + \gamma_1 + e_{\text{ph}} + e_{\text{Aug}}. \quad (1)$$

In the first step of the process, (1) an incident photon is absorbed by the Kr atom with emission of a slow electron e_{ph} from the deep $1s^2$ shell. Then the created $1s^{-1}$ vacancy decays with emission of a high-energy photon γ_1 and the creation of a $2p^{-1}$ vacancy in the intermediate $2p^6$ shell. In the next step, the $2p^{-1}$ vacancy decays by emission of the fast Auger electron e_{Aug}, leaving the doubly charged Kr^{2+} ion with two vacancies $3d^{-1}$ and $4p^{-1}$ in the outer shells.

We will study the process of the decay of the L_2 vacancy [the last step of reaction (1)], occurring via the Auger transi-

tion $L_2 - M_{4,5}N_{2,3}$; the energy of such transitions is located near $E_A^{(0)} \simeq 1610$ eV [15]. The energy of the photoelectron $E_{\text{ph}}^{(0)}$ at the moment of its generation is determined by the excess of photon energy above the $1s^{-1}$ threshold, $E_{\text{ph}}^{(0)} = \Delta E$. In our study, the excess photon energies are limited to 140 eV, hence the Auger electron is considerably faster than the photoelectron. The emitted fast Auger electron quickly passes the slower photoelectron and leaves the interaction region. The Coulomb repulsion between the electrons in the course of their relative motion additionally speeds up the Auger electron and slows down the photoelectron. This energy exchange leads to the PCI related distortion of the electron energy distributions. As a result, the maximum of the Auger energy spectrum E_A^{max} is blueshifted with respect to the Auger transition energy $E_A^{(0)}$ by $\varepsilon_A = E_A^{\text{max}} - E_A^{(0)} > 0$, while the maximum of the photoelectron energy spectrum is redshifted with respect to the excess photon energy ΔE by $\varepsilon_{ph} = E_{ph}^{\text{max}} - \Delta E < 0$. The target ion is too heavy to participate in this PCI energy exchange. Hence, due to energy conservation, $\varepsilon_A = -\varepsilon_{ph}$.

In the limit of a very large ratio of electron velocities, we can consider that the photoelectron position r_{ph} is essentially unchanged during the PCI with the fast Auger electron. In this case, the photoelectron undergoes shake-off at the moment of Auger decay due to the sudden change of its potential energy [1]. Before the Auger decay, the photoelectron moved in the field of a singly charged ion. After the Auger decay, when the Auger electron has left the interaction region, the photoelectron moves in the field of the doubly charged ion. The PCI energy shift in this classical picture equals the sudden change of the photoelectron potential energy, $\varepsilon_{\text{ph}} = -1/r_{\text{ph}}$.

For the theoretical description, we will use the semiclassical approach modified for CRAD processes [8]. This approach, based on the WKB approximation, treats quantum mechanically the coherent dynamics of all charged particles involved in the PCI. Among its advantages are applicability to a wide range of incident photon energies, including the near-threshold region, and flexibility that allows for descriptions of a wide variety of possible ionization channels. This approach was first developed [16–18] for the simplest ionization process when a deep inner-shell vacancy decays via a single Auger transition. It has then been extended to more complicated cascade channels of the primary vacancy decay including multi-Auger processes [19] and CRAD processes [8].

In the simplest case of single Auger decay, the amplitude of the ionization process is proportional to the overlap integral of the wave function of the intermediate state of the photoelectron propagating, prior to the Auger decay, in the field of the singly charged ion and the final wave function of the photoelectron moving in the field of the doubly charged residual ion and outgoing Auger electron [1]. Since the state of the ionized atom with an inner-shell vacancy is metastable, the emitted photoelectron in the intermediate state has the complex energy $E_{\text{ph}}^{(0)} = \Delta E + i\Gamma/2$, where Γ is the inner-shell vacancy decay width. Consequently, the photoelectron wave function exponentially decreases $\propto \exp(-\Gamma r_{\text{ph}}/v)$, where v denotes the photoelectron velocity. Therefore, the main contribution to the overlap integral comes from the electron distances about $r_{\text{ph}} \sim v/\Gamma$, which is quite natural because $v/\Gamma = v\tau$ is the free-electron path prior to the Auger decay, and $\tau = 1/\Gamma$ is the

Auger decay time. One can expect that the PCI energy shift should be given by the sudden change of the ionic potential at such electronic distances. Indeed, at high Auger electron velocity and rather large photon excess energies, where the semiclassical approximation is equivalent to the eikonal approximation [20], there is a simple analytical expression for the PCI energy shift $\varepsilon_{\mathrm{ph}} = -\Gamma/2v$ which confirms the physical picture of the PCI effect outlined above. The energy shift of the Auger electron line ε_A is opposite to the photoelectron shift.

Now, considering the CRAD processes, the model needs to take into account that the emission of the photon γ_1 in (1) does not change the charge state of the ion. So, the primary emitted photoelectron propagates in the field of the singly charged ion before the Auger decay during the time $\tau_{1s} + \tau_{2p}$ where $\tau_{1s} = 1/\Gamma_{1s}$ and $\tau_{2p} = 1/\Gamma_{2p}$ are the lifetimes of the $1s^{-1}$ and $2p^{-1}$ vacancies. The PCI energy exchange occurs at the moment of the Auger decay with $\tau_{1s} + \tau_{2p}$ delay after the $1s^2$ shell ionization. On these grounds, a model for the CRAD process has been proposed in Ref. [8], where its amplitude is given by the WKB amplitude for the single Auger decay [18] with an effective decay width corresponding to the $\tau_{1s} + \tau_{2p}$ lifetime:

$$\Gamma_{\mathrm{eff}} = \frac{1}{(\tau_{1s} + \tau_{2p})} = \frac{\Gamma_{1s}\,\Gamma_{2p}}{\Gamma_{1s} + \Gamma_{2p}}. \tag{2}$$

This model has been proven valid in cases [8,12] where it provided good agreement with experimental observations.

III. EXPERIMENT

The experiment was conducted at beamline 7-ID of Argonne's Advanced Photon Source [21] using a Scienta EW4000 hemispherical electron analyzer. The analyzer has a 200 mm mean radius and a multielement entrance lens for high collection efficiency and resolution over a broad range of electron energies. The analyzer was operated with a 1.5 mm entrance slit and 200 eV pass energy that gave an estimated electron energy resolution of 0.75 eV. The beamline's Si(111) double-crystal monochromator was used with the undulator's third harmonic. Horizontal and vertical slits defined the x-ray beam size to $\leqslant 1\ \mathrm{mm}^2$, and the estimated bandwidth was $\sim 1.6\ \mathrm{eV}$. A preliminary calibration of the x-ray energies was obtained by measuring the Kr K-shell x-ray absorption spectrum near 14.3 keV [22].

The x rays passed through a gas cell positioned at the source point of the electron analyzer with its entrance lens parallel to the linear polarization plane of the x-ray beam. Krypton flowed through the gas cell at constant density and electrons exited through a slit facing the analyzer's entrance lens. A comprehensive experimental and theoretical study of Kr L-shell Auger transitions is given in Ref. [15]. The $L_2 - M_{4,5}N_{2,3}$ Auger transition near $\sim 1610\ \mathrm{eV}$ was chosen for investigation of PCI effects because it is relatively well isolated from other transitions and its multiline substructure is calculated (see the Supplemental Material of Ref. [15].)

Below the K edge, the Auger line is generated by direct L_2 photoionization. Above the K edge, the yield of the $L_2 - M_{4,5}N_{2,3}$ Auger line was observed to increase by $\times 10$. This is due to L_2 vacancies generated by K-shell photoionization

followed by KL_2 x-ray emission. Fluorescence yields of K vacancies increase rapidly with atomic number Z, and the fluorescence yield of Kr is 0.643 [11]. X-ray emission transfers the K vacancies to L and M subshells, and approximately 30% of the radiative transfers are to the L_2 subshell [23]. Since the L_2 vacancy state has a total angular momentum $J = 1/2$ and equally populated magnetic substates, it cannot be aligned [2]. The $L_2 - M_{4,5}N_{2,3}$ Auger electrons are therefore ejected isotropically.

To investigate PCI effects, which strongly depend on the $1s$ photoelectron excess energy, the Auger electron spectrum was measured from the $1s$ ionization threshold to several-hundred-eV excess energy. The position of the Kr $1s$ ionization threshold is obscured in the x-ray absorption spectrum by lifetime broadening of the $1s \to np$ Rydberg series and the arctangent shape of the ionization edge [22]. We determined the ionization threshold accurately by recording the $L_2 - M_{4,5}N_{2,3}$ Auger electron spectrum while stepping the x-ray energy through the pre-edge resonances. This produced resonant Auger transitions that are shifted in electron energy from the diagram transition. A full report on the analysis of the resonant Auger transitions is in preparation [24]. One of the results is an accurate determination of the $1s$ ionization threshold. Briefly, KL_2 x-ray emission at the $1s \to 5p$ resonance produces the $2p^{-1}5p$ intermediate state that decays to the $3d^{-1}4p^{-1}5p$ final state. The integrated peak intensity of this final state displays a maximum at the position of the $1s \to 5p$ resonance. Using the $Z + 1$ approximation to link the $1s \to np$ Rydberg series of Kr to the corresponding optical spectrum of Rb [25], the $1s$ ionization energy is 2.61(1) eV above the $5p$ resonance. The $Z + 1$ term value is consistent with the analysis of the Kr x-ray absorption spectrum [22] and with the Kr $3d^{-1}np$ Rydberg series recorded in high-resolution electron impact measurements [26]. With this procedure, we located the position of the Kr $1s$ ionization threshold (14327.19(13) eV [27]), and therefore the excess energies, with an accuracy of better than 50 meV.

IV. RESULTS OF MEASUREMENTS AND CALCULATIONS

The results of our experimental measurements and theoretical calculations on the $L_2 - M_{4,5}N_{2,3}$ Auger electron emission are presented in Figs. 1–3. In Fig. 1, we show the detailed analysis of the Auger spectrum formation at $\Delta E = 4\ \mathrm{eV}$ excess of photon energy above the $1s$ ionization threshold. In Fig. 2, we compare the measured Auger line shapes with two kinds of theoretical spectra calculated for three values of $\Delta E = 2, 10, 95\ \mathrm{eV}$. One theoretical line shape is calculated taking into account the most intense partial contributions of $L_2 - M_{4,5}N_{2,3}$ Auger transitions, and another shows the partial contribution of the main Auger transition only. In Fig. 3, we compare the experimental and theoretical results for the PCI energy shift of the Auger spectra within the wide range of photon excess energies $0\ \mathrm{eV} < \Delta E < 140\ \mathrm{eV}$. All of the Auger spectra presented demonstrate the presence of PCI energy distortion which manifests itself in prominent asymmetry of the line shape and energy shift of its maximum. The PCI effects are most prominent at small excess energies and diminish at large ΔE values.
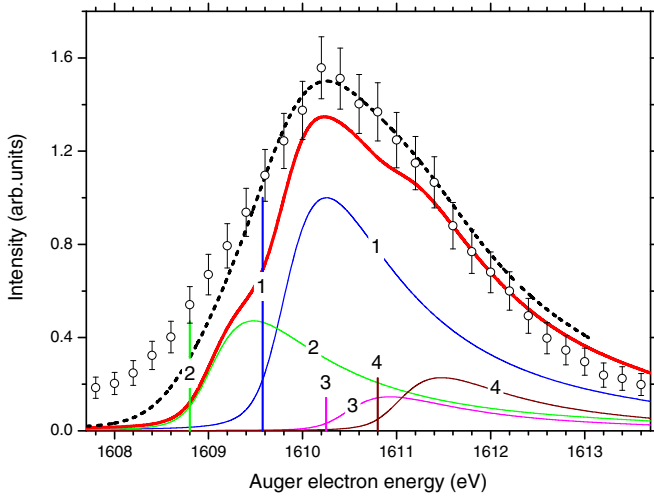
FIG. 1. Calculated line shape of the $L_2 - M_{4,5}N_{2,3}$ Auger transition at $\Delta E = 4$ eV photon excess energy above the $1s$ ionization threshold. Thin colored lines marked as 1–4 show contributions of individual transitions (see text). Thick vertical lines show the locations of these lines and their relative strengths. The thick red line shows the summed calculated line shape and the dashed line presents this intensity convolved with the electron detector resolution function. The black open circles present the measured spectrum at the same energy.

The $L_2 - M_{4,5}N_{2,3}$ Auger spectrum is formed by the contributions of 12 closely spaced Auger transitions to the final ionic states with two vacancies, $3d^{-1}$ and $4p^{-1}$, having different terms and total angular momenta [15] (see Supplemental Material to Ref. [15]). The energies and relative intensities of the most intense transitions, which carry more than 90% of the total $L_2 - M_{4,5}N_{2,3}$ Auger intensity are shown in Fig. 1 by thick vertical color lines marked with numbers. The intensity of the strongest Auger line 1 we take as one unit. The energy of this Auger transition has been taken equal to $E_A^{(0)} = 1609.576$ eV to match the maximum E_A^{max} of the measured $L_2 - M_{4,5}N_{2,3}$ Auger transition line shape at the excess of photon energy of 1696 eV where the PCI shift becomes negligible. The relative intensities and the energy spacings of the other strong individual Auger transitions have been taken according to Ref. [15]. The second Auger line 2 is shifted by -0.8 eV from line 1 and has the relative intensity equal to 0.472. Two very close transitions with the energy difference of 0.1 eV, which we will consider for the sake of simplicity as one transition number 3, have the summed relative intensity equal to 0.146. This line is shifted by $+0.65$ eV from the main line 1. The transition number 4 is shifted by $+1.2$ eV from line 1 and has the relative intensity equal to 0.228.

The spectra of Auger emission have been calculated according to the following scheme. First the PCI-distorted line shapes have been calculated for all four individual Auger transitions within the modified quasiclassical approach [8], i.e., using the Auger decay amplitude of Ref. [18] with the effective width Γ_{eff} in Eq. (2). For the values of the inner shell vacancy widths, $\Gamma(1s^{-1}) = 2.75$ eV, $\Gamma(2p_{1/2}^{-1}) = 1.31$ eV [11], Eq. (2) gives the value of $\Gamma_{eff} = 0.89$ eV. The intensities of the partial Auger lines have been calculated in

arbitrary units and are proportional to the relative intensities of the corresponding Auger transitions.

Then the obtained partial Auger spectrum contributions were broadened to take into account that the final ionic states of the Auger transitions $L_2 - M_{4,5}N_{2,3}$ have a finite lifetime τ_f, leading to a spread in energy following a Lorentzian distribution with width $\Gamma_f = 1/\tau_f$. Hence, the energies of the emitted Auger electrons, in addition to the PCI effect, must also be affected by this energy distribution, and the correct description of the Auger spectrum requires an additional convolution of the calculated PCI distorted Auger spectrum with a Lorentzian of width Γ_f [2,28,29]. In this paper, the value of Γ_f was chosen to be 88 meV, which is equal to the width of the $3d^{-1}$ single core-hole state [30]. Hence the theoretical partial line shapes were convoluted with a Lorentzian of full width at half maximum (FWHM) $= 88$ meV that simulates the spread of the $Kr^{2+}(3d^{-1}4p^{-1})$ state energy. Calculated by this procedure, the four partial contributions are shown in Fig. 1 by thin colored solid lines marked with corresponding numbers.

We note a strong blueshift of $\varepsilon_A = 0.65$ eV for all calculated partial Auger spectra from the corresponding unshifted Auger transition energies and their remarkable asymmetrical line shapes, namely the right wing of the Auger line shape decreases more slowly than the left one. As expected, the observed strong PCI distortion is connected with the large values of the K and L_2 vacancy widths.

The total contribution of all four partial Auger lines is shown in Fig. 1 by the thick solid red line. It also demonstrates the PCI related asymmetry, similar to each individual partial contribution, but its line shape is much more complicated than the partial spectra as a result of their combined contributions. The FWHM of the total Auger spectrum is much larger than the widths of the component lines, but its maximum almost coincides with the maximum of line 1 because it provides the largest contribution to the total spectrum.

Finally, to compare with the measurements, the line shapes obtained were convoluted with a Gaussian of FWHM $= 750$ meV that simulates the total experimental resolution function of the electron analyzer. The spectral profile calculated in this way is presented in Fig. 1 by the black dashed line. Since the intensities of the Auger emission are measured and calculated in arbitrary units, we chose arbitrary units to adjust their maximum values. There is some discrepancy between the positions of the maxima of the experimental and theoretical spectra, as shown in Fig. 3, and this complicates the comparison of the observed and calculated line shapes. For the sake of visual convenience, we shift in Fig. 1 the calculated spectrum (black dashed line) by -0.14 eV to match the position of the maximum of the experimental spectrum. The observed agreement between the experimental and theoretical line shapes supports the validity of the theoretical model. There is a small disagreement between the measured and calculated line shapes at the left profile wing in the energy region below 1609 eV. In this energy region, the measurements and calculations from Ref. [15] predict small contributions from the $L_1 - M_1N_{2,3}$ and the $L_2M_{4,5} - M_{4,5}M_{4,5}N_{2,3}$ Auger transitions. This can explain the higher background and slight misfit between experiment and theory. Small contributions from these Auger transitions can also explain discrepancies between the measured and calculated line
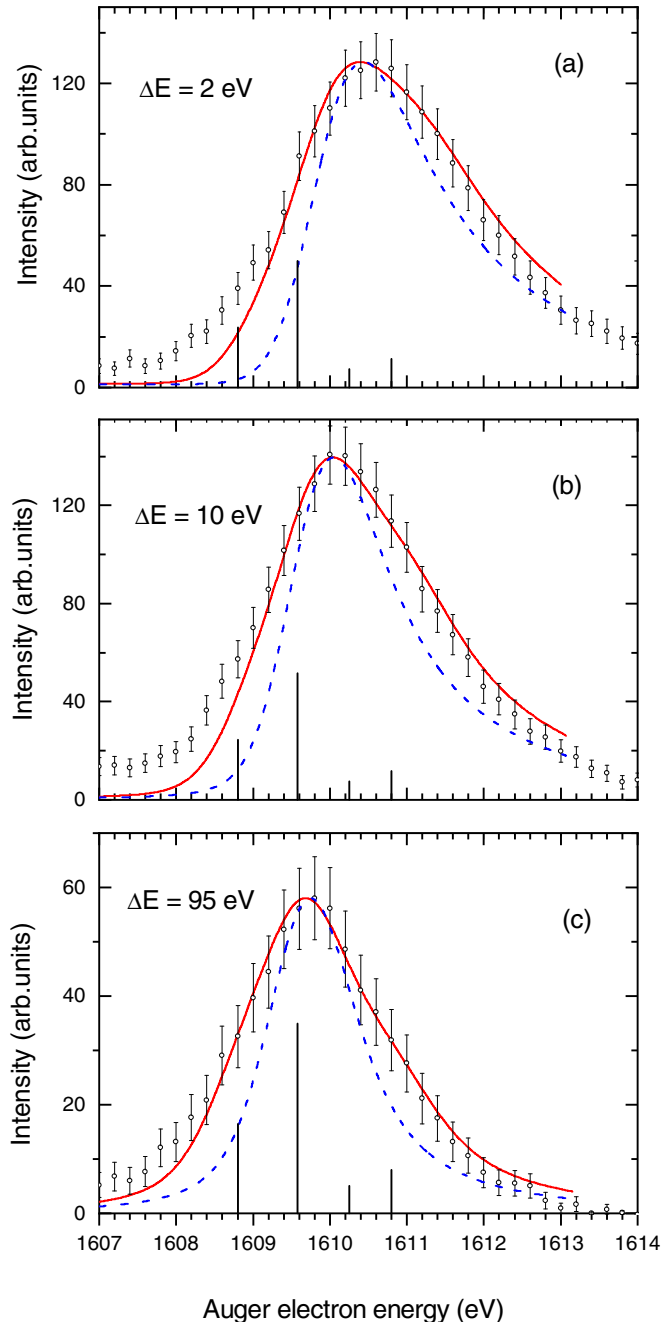
FIG. 2. Line shapes of the $L_2 - M_{4,5}N_{2,3}$ Auger transition at different photon excess energies above the $1s$ ionization threshold: (a) $\Delta E = 2$ eV, (b) $\Delta E = 10$ eV, (c) $\Delta E = 95$ eV. The red solid lines show the calculated spectra accounting for contributions from four individual lines (see text) and the blue dashed lines present the calculated line shapes accounting for the contribution of the main line 1 only. The black circles show the measured spectra. The black vertical lines show the positions of the unshifted individual lines.
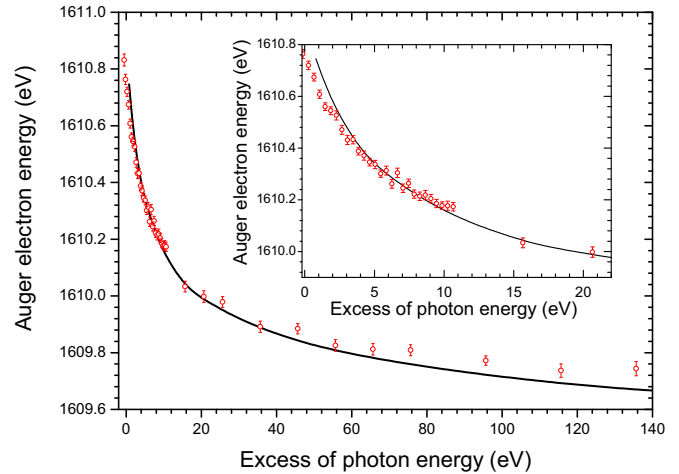
FIG. 3. Energies $E_{\mathrm{Aug}}^{\max}$ of the maximum of the $L_2 - M_{4,5}N_{2,3}$ Auger line versus the photon excess energy ΔE above the $1s$ ionization threshold. The black line presents the calculated values and red open circles show the measured energies. The inset graph shows the results close to threshold.

are calculated as described above that combine the contributions of four Auger lines. The second curves, shown by the dashed blue lines, result from the same calculations but account for the contribution of the main Auger line 1 only. Thus the difference between these two theoretical curves demonstrates the need to include the contributions of the secondary Auger lines. Similar to the curves in Fig. 1, all Auger profiles have been normalized for the same maximal intensity. Also, the calculated curves in Fig. 2 have been shifted by values ranging from 30 to 180 meV to match the energy positions of the experimental curves for visual comparisons of the line shapes. The observed discrepancies in the positions of the experimental and theoretical maxima of Auger profiles as a function of the excess photon energy can be seen in Fig. 3 and are discussed below. The discrepancies between the measured and calculated line shapes can be attributed to uncertainties in the experimental calibration of the energy scale, as well as to some uncertainties in the calculated positions of the individual lines. Note that similar disagreement between the measured and calculated line shapes was observed earlier in Ar $1s$ photoionization followed by single Auger decay [3].

The PCI distortion of the Auger spectra presented in Fig. 2 is clearly seen in the line-shape asymmetry and in the energy shift of the maximum compared with the unshifted position of the main Auger transition indicated by the vertical black line. The line-shape distortion increases as the excess photon energy ΔE decreases toward the threshold. The maxima positions of the two calculated curves almost coincide because the main Auger transition gives the leading contribution to the spectra (see Fig. 1). Hence, the PCI energy shift of the $L_2 - M_{4,5}N_{2,3}$ Auger spectrum can be well described by taking into account the main Auger line only (see Fig. 3). However, the single line profiles do not agree satisfactorily with the measured Auger line shapes, neither for small ΔE nor for the region of large ΔE. That is, the calculated line shapes of the main Auger transition are significantly narrower than the measured profiles. On the other hand, the calculated

shapes presented in Fig. 2 for the other excess photon energies (see below).

In Fig. 2, we compare the experimental and calculated Auger spectra for three excess photon energies, $\Delta E = 2$, 10, 95 eV. There we plot two theoretical curves for each excess photon energy. The first curves, shown by the solid red lines,

line shapes of the total Auger spectrum shows rather reasonable agreement with the measured profiles. For small ΔE, they reflect the PCI distortion, whereas for large ΔE the calculated profiles are rather symmetrical; their widths are also in reasonable agreement with the widths of the measured line shapes. Hence both the PCI distortion and the contributions from several overlapping Auger lines form the observed line shape in the case of the $L_2 - M_{4,5}N_{2,3}$ Auger transition.

In Fig. 3, the measured and calculated energies $E_{\mathrm{Aug}}^{\max}$ of the maximum of the $L_2 - M_{4,5}N_{2,3}$ line are presented as a function of the excess photon energy region $0 < \Delta E < 140$ eV. The shift ε_A of the $E_{\mathrm{Aug}}^{\max}$ from its unshifted value, $E_A^{(0)} = 1609.576$ eV, is mainly associated with the PCI distortion. The smaller the excess photon energy ΔE is above threshold, the larger is the PCI shift ε_A of the Auger line. Both the measured and calculated dependencies of the line shift ε_A on the excess energy ΔE show similar behavior. For small values of excess photon energy 1 eV $< \Delta E < 4$ eV, the shift is in the range 0.8 eV $< \varepsilon_A < 1.1$ eV. Such rather large values of the PCI energy shift are caused by the large widths of the K and L_2 vacancies. The shifts calculated for Auger line 1 alone and for the total Auger spectrum almost coincide. For the entire region, a reasonable agreement of the measured and calculated values is found, although at small excess photon energies $\Delta E \leqslant 5$ eV the measured shift is slightly smaller than the calculated one.

It should be noted that inner-shell photoionization of the Kr atom followed by the CRAD process similar to Eq. (1) has recently been studied in Ref. [13]. In that work, the Auger transition $L_3 - M_{4,5}M_{4,5}$ was investigated instead of the $L_2 - M_{4,5}N_{2,3}$ Auger transition considered in the present paper. One of the goals of Ref. [13] was to compare PCI effects recorded above the L_3 edge but below the K edge, where one-step Auger decay from the L_3-vacancy state occurs, to PCI effects recorded above the K edge where a time delay due to KL_3 fluorescence plays a role. Differences in the line shapes for the two cases were observed, and a theoretical model was proposed that explains the measured PCI-distorted line shapes. However, Ref. [13] also reported deviations from the effective lifetime model in Eq. (2) that explains the PCI-distorted $L_2 - M_{4,5}N_{2,3}$ Auger line shapes and peak shifts measured in the present paper fairly well.

We have analyzed the discrepancies of our work with Ref. [13] by comparing PCI energy shifts at similar excess energies. We find that the discrepancies are caused by the difference of detector resolutions and by the effects of photoelectron recapture discussed in Ref. [3]. In Ref. [13], measured Auger electron spectra were reported at three excess energies above the $1s$ ionization threshold, 0.6 eV, 5.6 eV, and 95.6 eV. In Ref. [13], the measured line shapes of the electron spectra are compared with theory in Fig. 2 and the PCI shifts are compared with theory in Fig. 5. The excess energy of 5.6 eV is high enough so photoelectron recapture is not involved, and our model based on the semiclassical (WKB) amplitude of Ref. [18] works pretty well. For comparison of the calculated Auger spectrum with the experimental one, the calculated spectrum should be convoluted with a Gaussian function that accounts for the detector resolution. For the detector resolution of 0.75 eV FWHM used in the present paper and 0.4 eV FWHM used in Ref. [13], we obtain PCI

energy shifts of 0.735 eV and 0.6 eV, respectively, at 5.6 eV excess energy. These shifts agree well with the measurements of 0.73 eV and 0.58 eV, respectively. The effective decay width of 0.9 eV for $L_3 - M_{4,5}M_{4,5}$ Auger transitions used in Ref. [13] almost coincides with our effective width of 0.89 eV used for the $L_2 - M_{4,5}N_{2,3}$ Auger transition. The two studies are therefore consistent and the apparent difference is caused by the different detector resolutions.

The situation at 0.6 eV excess energy is quite different because here the PCI energy shift is larger than the photon excess energy. Photoelectron recapture by the ion takes place and the WKB approach does not work properly. While the WKB amplitude [18] accounts for the localized electron states, it does not account for the discrete nature of the electron spectrum but treats it as continuous. Hence, the fine structure of the electron spectrum is described as a rough average. Therefore, the agreement with experimental data strongly depends on the detector resolution. In the present paper, with a detector resolution of 0.75 eV, the calculated PCI energy shift systematically overestimates the experimental shift at low excess energies as shown in Fig. 3 and discussed earlier. Nevertheless, at 0.6 eV excess energy, our calculated PCI energy shift is 1.15 eV while the experimental shift is 1.1 eV.

We note that with a detector resolution of 0.4 eV, the 0.6 eV excess-energy spectrum in Fig. 2 of Ref. [13] shows a distinct structure that could result from photoelectron recapture. We suggest that this can explain apparent disagreement with the predictions of the effective width model. In Fig. 5 of Ref. [13], the PCI energy shift measured at the detector resolution of 0.4 eV is 0.76 eV while the effective width model predicts 1.07 eV shift. This discrepancy is six times larger than the discrepancy between the effective width model and experiment observed at the detector resolution of 0.75 eV and at the same excess photon energy of 0.6 eV reported in the present paper. Note that the theoretical approach developed for the CRAD process in Ref. [13] also does not account for the discrete spectrum of localized photoelectron states and therefore does not reproduce the structure of the 0.6 eV excess-energy spectrum and overestimates its PCI energy shift.

Photoelectron recapture and experimental resolution are factors that complicate comparisons of models of PCI-distorted Auger electron line shapes at low excess energies and more theoretical efforts are needed to reproduce details in the measured spectra near the photoionization threshold.

V. CONCLUSION

We have reported on PCI effects for the case of Kr K-shell photoionization in which the initially created K vacancies are transferred to the L_2 subshell by x-ray emission and the L_2 holes decay by an $L_2 - M_{4,5}N_{2,3}$ Auger process. Electron spectroscopy with tunable x rays was used to record the Auger electron spectra from the K-shell ionization threshold to several-hundred eV excess energy. The Auger-electron peaks were observed to increasingly shift in energy and become increasingly asymmetric as the excess energy approaches the threshold due to energy exchanges with the $1s$ photoelectrons. The PCI effects were modeled using a semiclassical approach modified to account for the lifetimes of the K- and L_2- hole

states. By including several closely spaced $L_2 - M_{4,5}N_{2,3}$ Auger transitions with different final-state terms and angular momenta, the experimental line shapes were well reproduced. The energy shifts of the Auger electrons as a function of excess energy matched the experimental shifts fairly well. We conclude that the theoretical approach contains the essential elements to model this class of deep inner-shell decays that begin with an x-ray emission step. Such processes are particularly strong in the K-shell vacancy decays of heavy atoms.

[1] M. Yu. Kuchiev and S. A. Sheinerman, Sov. Phys. Usp. **32**, 569 (1989).

[2] V. Schmidt, *Electron Spectrometry of Atoms using Synchrotron Radiation* (Cambridge Press, Cambridge, UK, 1997).

[3] R. Guillemin, S. Sheinerman, R. Püttner, T. Marchenko, G. Goldsztejn, L. Journel, R. K. Kushawaha, D. Céolin, M. N. Piancastelli, and M. Simon, Phys. Rev. A **92**, 012503 (2015).

[4] S. Sheinerman, P. Lablanquie, F. Penent, Y. Hikosaka, T. Kaneyasu, E. Shigemasa, and K. Ito, J. Phys. B: At. Mol. Opt. Phys. **43**, 115001 (2010).

[5] F. Penent, S. Sheinerman, L. Andric, P. Lablanquie, J. Palaudoux, U. Becker, M. Braune, J. Viefhaus, and J. H. D. Eland, J. Phys. B: At. Mol. Opt. Phys. **41**, 045002 (2008).

[6] S. Sheinerman, P. Lablanquie, F. Penent, J. Palaudoux, J. H. D. Eland, T. Aoto, Y. Hikosaka, and K. Ito, J. Phys. B: At. Mol. Opt. Phys. **39**, 1017 (2006).

[7] S. Sheinerman, P. Linusson, J. H. D. Eland, L. Hedin, E. Andersson, J.-E. Rubensson, L. Karlsson, and R. Feifel, Phys. Rev. A **86**, 022515 (2012).

[8] R. Guillemin, S. Sheinerman, C. Bomme, L. Journel, T. Marin, T. Marchenko, R. K. Kushawaha, N. Trcera, M. N. Piancastelli, and M. Simon, Phys. Rev. Lett. **109**, 013001 (2012).

[9] C. Bomme, R. Guillemin, S. Sheinerman, T. Morin, L. Journel, T. Marchenko, R. K. Kushawaha, N. Trcera, M. N. Piancastelli, and M. Simon, J. Phys. B: At. Mol. Opt. Phys. **46**, 215101 (2013).

[10] P. Lablanquie, S. Sheinerman, L. Andric, J. Palaudoux, Y. Hikosaka, K. Ito, and F. Penent, J. Electron. Spectrosc. Relat. Phenom. **185**, 198 (2012).

[11] M. O. Krause, J. Phys. Chem. Ref. Data **8**, 307 (1979).

[12] S. Kosugi, R. Guillemin, O. Travnikova, T. Marchenko, D. Koulentianos, J. B. Martins, F. Hosseini, R. Püttner, D. Céolin, L. Journel, M. N. Piancastelli, I. Ismail, F. Koike, M. Iizawa, S. Sheinerman, L. Gerchikov, Y. Azuma, and M. Simon (unpublished).

[13] S. Kosugi, F. Koike, M. Iizawa, M. Oura, T. Gejo, K. Tamasaku, J. R. Harries, R. Guillemin, M. N. Piancastelli, M. Simon, and Y. Azuma, Phys. Rev. Lett. **124**, 183001 (2020).

[14] M. O. Krause and J. H. Oliver, J. Phys. Chem. Ref. Data **8**, 329 (1979).

[15] N. Boudjemia, K. Jänkälä, T. Gejo, Y. Kohmura, M. Huttula, M. N. Piancastelli, M. Simon, M. Oura, and R. Püttner, Phys. Rev. A **104**, 012804 (2021).

[16] A. Niehaus, J. Phys. B: At. Mol. Phys. **10**, 1845 (1977).

[17] K. Helenelund, S. Hedman, L. Asplund, U. Gelius, and K. Siegbahn, Phys. Scr. **27**, 245 (1983).

[18] P. Straten, R. Morgenstern, and A. Niehaus, Z. Phys. D **8**, 35 (1988).

[19] L. Gerchikov and S. Sheinerman, Phys. Rev. A **84**, 022503 (2011).

[20] M. Yu. Kuchiev and S. A. Sheinerman, Sov. Phys. JETP **63**, 986 (1986).

[21] D. A. Walko, B. W. Adams, G. Doumy, E. M. Dufresne, Y. Li, A. M. March, A. R. Sandy, J. Wang, H. Wen, and Y. Zhu, in *Proceedings of the 12th International Conference on Synchrotron Radiation Instrumentation–SRI2015*, AIP Conf. Proc. No. 1741, edited by Q. Shen and C. Nelson (AIP, New York, 2016), p. 030048.

[22] M. Breinig, M. H. Chen, G. E. Ice, F. Parente, B. Crasemann, and G. S. Brown, Phys. Rev. A **22**, 520 (1980).

[23] J. B. Kortright and A. C. Thompson, in *X-Ray Data Booklet*, 3rd ed. (Lawrence Berkeley National Laboratory, University of California, Berkeley, 2009).

[24] S. Li, D. Koulentianos, S. H. Southworth, G. Doumy, L. Young, D. A. Walko, R. Püttner, J. D. Bozek, D. Céolin, A. Verma, R. Guillemin, M. N. Piancastelli, M. Simon, L. G. Gerchikov, and S. A. Sheinerman (unpublished).

[25] A. Kramida, Yu. Ralchenko, J. Reader, and NIST ASD Team (2021), NIST Atomic Spectra Database (ver. 5.9), National Institute of Standards and Technology, Gaithersburg, MD, https://physics.nist.gov/asd (accessed June 27, 2022); https://doi.org/10.18434/T4W30F.

[26] G. C. King, M. Tronc, F. H. Read, and R. C. Bradford, J. Phys. B: At. Mol. Phys. **10**, 2479 (1977).

[27] R. D. Deslattes, E. G. Kessler, Jr., P. Indelicato, L. de Billy, E. Lindroth, and J. Anton, Rev. Mod. Phys. **75**, 35 (2003).

[28] W. Mehlhorn, in *Atomic Inner-Shell Physics*, edited by B. Crasemann (Plenum, New York, 1985), p. 119.

[29] G. B. Armen, H. Aksela, T. Aberg, and S. Aksela, J. Phys. B: At. Mol. Opt. Phys. **33**, R49 (2000).

[30] M. Jurvansuu, A. Kivimäki, and S. Aksela, Phys. Rev. A **64**, 012502 (2001).